Available online at www.sciencedirect.com

ScienceDirect

Advances in Space Research 69 (2022) 2197–2209

ADVANCES IN SPACE RESEARCH
(a COSPAR publication)

www.elsevier.com/locate/asr

Collision avoidance control for formation flying of multiple spacecraft using artificial potential field

Jiyoon Hwang, Jinah Lee, Chandeok Park *

Department of Astronomy, Yonsei University, Seoul 03722, Republic of Korea

Received 8 June 2021; received in revised form 6 November 2021; accepted 6 December 2021
Available online 10 December 2021

Abstract

This study presents trajectory design/control for spacecraft formation flying with obstacle avoidance. Based on the artificial potential field (APF), a formation potential is first defined to derive a formation control law for virtual structure, which enables multiple spacecraft to maintain polygonal or tetrahedral formation. As an efficient method to circumvent local minima which often occur in the APF-based approach, a *newly* proposed rotational potential is derived in a local coordinate frame to add in the APF framework. The synthesized formation and rotational potential function is used to develop a gradient-based control law to design/control the formation flying trajectory while avoiding collision with obstacles. Proven to be asymptotically stable in the sense of Lyapunov, the proposed continuous feedback control law is demonstrated via formation keeping/reconfiguration examples. The proposed approach successfully maintains the trajectory in the desired formation without colliding with obstacles and without falling into local minimum. These results are comparatively analysed with those of other APF-based approaches. The overall analysis shows that the proposed rotational potential, which has been newly derived in this research, enables a group of spacecraft in formation to efficiently avoid collision with obstacles without convergence to a local minimum.

Keywords: Artificial Potential Field (APF); Autonomous Control; Collision Avoidance; Spacecraft Formation Flying

1. Introduction

A group of spacecraft in a rigorously coordinated formation can perform demanding missions that are difficult to achieve with a single spacecraft (Bandyopadhyay et al., 2016, Burch et al., 2016). One example is NASA's Magnetospheric Multiscale (MMS) mission in which four spacecraft fly in a tetrahedral shape (Burch et al., 2016). Applications with spacecraft formation flying have motivated even unmanned aerial vehicles (UAV), robots, and autonomous underwater vehicles to employ coordinated formation maneuvers (Balch and Arkin, 1998, Fu et al., 2020, Giulietti et al., Pham et al., 2018, Ren and Sorensen, 2008, Stilwell and Bishop, 2000, Wu et al., 2020).

The trajectory/position control of formation flying with collision avoidance has been achieved by a variety of approaches such as virtual structure, behavioural approach, and leader–follower approach (Beard et al., 2001, Chai et al., 2019, Cheng et al., 2020, Rezaee and Abdollahi, 2013, Rouzegar et al., 2021, Scharf et al., 2004, Wang et al., 2020, Yang et al., 2021). For example, Rezaee and Abdollahi (2014) proposed to integrate the virtual structure approach and the behavioural approach in two-dimensional space. A virtual leader is positioned at the center of a circle with robots located equidistantly on the circle. As the robots approach obstacles, they initiate avoiding them by the behavioral approach, adjusting the shape of formation. As this approach is intuitive and

* Corresponding author.
E-mail addresses: amoearth@yonsei.ac.kr (J. Hwang), jinajina92@gmail.com (J. Lee), park.chandeok@yonsei.ac.kr (C. Park).

https://doi.org/10.1016/j.asr.2021.12.015
0273-1177/

useful, it was applied only in two-dimensional space. Chang et al. (2016) expanded Rezaee's strategy of collision-free formation control into three-dimensional space so that UAVs could fly in formation without collision. Recently, Silvestrini and Lavagna (2021) applied Artificial Neural Networks (ANNs) to formation control. They employed an online Radial-Basis Function Neural Network (RBFNN) to approximate dynamical terms embracing nonlinearities and increased the control accuracy of an Artificial-Potential-Field (APF) based controller.

Many spacecraft formation flying missions make it necessary to avoid collision while maintaining formation (Hu et al., 2015, Liu et al., 2018). The APF is a well-known obstacle avoidance technique in which its gradient works as an actuating force (Cao et al., 2018, Chu et al., 2016, Khatib, 1986, Li et al., 2018, Starek et al., 2016, Steindorf et al., 2017). A repulsive and an attractive potential fields are *artificially* formed around the obstacles and targets, respectively, so that spacecraft reach the target while avoiding obstacles through the gradient of the integrated potential field. Since the positions of obstacles are expressed as an explicit function, feedback controls can be configured by reflecting the states of obstacles in real-time with relatively low computational burden (Khatib, 1986).

Though intuitive and useful, the APF often leads to undesirable 'local minima' when the attractive and the repulsive potentials are combined to produce an unintended equilibrium before reaching the target. Goals Non-reachable with Obstacles Nearby (GNRON) problem can also happen, as spacecraft cannot reach the target point because of the repulsive force generated from obstacles nearby. Some algorithms have been proposed to address this issue (Badawy and McInnes, 2008, Rostami et al., 2019). Badawy and McInnes (2008) applied a superquadric function to a repulsive potential of the APF; as a spacecraft gradually comes closer to an obstacle, the repulsive potential is adjusted to represent the actual shape of the obstacle rather than a hyper ellipse. This approach with the superquadric function can lower the incidence of falling into the local minima, though a spacecraft cannot escape from the local minima if it is co-aligned symmetrically with obstacles and targets in a straight line. This approach can also secure a wider range of flight space. Rezaee and Abdollahi (2013) presented a new approach for obstacle avoidance by designing a rotational force function in two-dimensional space, which leads the robot to detour the obstacle rather than to move in its opposite direction. While the virtual target approach (for example, with a superquadric function) is the safest to avoid falling into the local minima, it is rather unclear how to systematically set the virtual target. The rotational force function can be a simple yet effective way free from local minima, however, it has not been synthesized in a APF-based controller for analysing stability. It is also challenging to implement rotational force function in general three-dimensional space. Although Chang et al. (2016) derived rotational force vector in three-dimensional space for UAVs, the stability of controller is not guaranteed when it comes to collision avoidance maneuver. These survey suggests that: if a rotational *potential* can be obtained from the rotational force function to be integrated into the APF, the resultant controller can be asymptotically stable, avoid convergence to local minima, while taking advantage of their simple and intuitive formulation.

This research presents an algorithm for designing/controlling trajectories of multiple spacecraft in formation while avoiding collision. Motivated by Rezaee and Abdollahi (2013), a new kind of APF for formation flying with collision avoidance is proposed, and a newly derived rotational *potential*, which prevents spacecraft from being stuck at a local minimum, is presented in a local *3-dimensional* coordinate frame. We first integrate the APF and the rotational potential into one single function for compact expression and derivational convenience. Once they are synthesized to build a control law for designing/-controlling formation flying trajectories while avoiding collision, it is first proven to be asymptotically stable in the sense of Lyapunov. Numerical simulations demonstrate the performance and effectiveness of the proposed control law through formation keeping/reconfiguration examples; the proposed algorithm achieves the control objectives for formation flying and collision avoidance, while mitigating the convergence to a local minimum thanks to the rotational potential. Only the formations of regular polygons/tetrahedron are considered for a group of spacecraft flying in coordination. It is assumed that spacecraft can communicate with each other instantly and can detect obstacles in advance.

The rest of this research is structured as follows. Section 2 presents the dynamical equations of motion. In Section 3, the enhanced potential functions and the associated control laws for formation flying are derived based on the APF and the virtual structure. Section 4 mainly discusses our newly proposed collision avoidance technique and the associated gradient-based control law for collision avoidance. In Section 5, numerical simulations demonstrate successful applications of the developed control law to some non-trivial formation flying examples. Section 6 summarizes and concludes the whole discussion.

2. Dynamical equations of motion

Consider Hills-Clohessy-Wiltshire (HCW) linearized dynamics to describe the relative motion of spacecraft near Earth (Chu et al., 2016, Li et al., 2018):

$$\begin{aligned} \ddot{x} &= 2w_0\dot{y} + 3w_0^2x, \\ \ddot{y} &= -2w_0\dot{x}, \\ \ddot{z} &= -w_0^2z \end{aligned} \tag{1}$$

where the x-axis is along the radial direction from the Earth center to the chief spacecraft, the z-axis is normal to the orbital plane, and the y-axis completes the right-hand coordinates (Fig. 1). w_0 is the angular frequency of the chief.

$$w_0 = \sqrt{\frac{\mu}{a_c^3}} \tag{2}$$

where a_c is the orbital radius of the chief spacecraft, $\mu = GM_E$ is the gravitational parameter, G is the gravitational constant and M_E is the mass of the Earth. The equations of motion with the control input are stated in vector form as:

$$\begin{aligned} \ddot{\boldsymbol{r}} &= f(\boldsymbol{r}, \dot{\boldsymbol{r}}) + \boldsymbol{u}, \\ f(\boldsymbol{r}, \dot{\boldsymbol{r}}) &= \left[2w_0\dot{y} + 3w_0^2 x, -2w_0\dot{x}, -w_0^2 z\right]^T, \\ \boldsymbol{r} &= [x, y, z]^T, \boldsymbol{u} = \left[u_x, u_y, u_z\right]^T \end{aligned} \tag{3}$$

where $\boldsymbol{r}$ is the relative radius of the deputy spacecraft.

3. Artificial potential function (APF) for spacecraft formation flying

As a kind of path planning technique, the APF artificially constructs a potential field in a given configuration space such that it becomes zero at the target (goal) point. Its gradient acts as actuating force to move a spacecraft in the direction of decreasing the potential to zero (Lee et al., 2015). As mentioned in the introduction, this research considers a group of spacecraft maintaining polygonal or tetrahedral shapes only. Two types of potential functions are defined for polygonal/tetrahedral formation flying; the first one is a structural potential which places a spacecraft on a circle/sphere with arbitrary radius R; the second one is a repulsive potential which maintains the desired distance between the spacecraft on the circle/sphere. Before defining the structural potential, a (non-existent) virtual leader is assumed to be located at the center of the circle/sphere to maintain a rigid formation. The virtual leader guides the movement of the entire spacecraft in formation, and the actual spacecraft keep equidistant from all the other spacecraft on the circle/sphere. The trajectory of the virtual leader acts as a reference trajectory that all the spacecraft track in our algorithm and should be designed/represented in advance with respect to the HCW-frame.

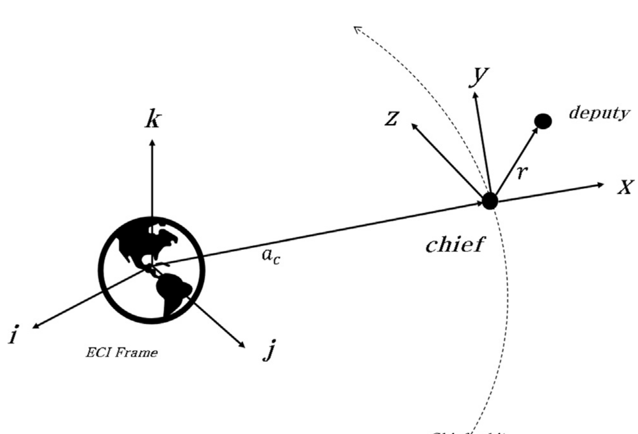

Fig. 1. ECI and relative coordinate frames.

To locate multiple spacecraft on the sphere, a positive definite structural potential of the k-th spacecraft ($k \in \{1, 2, \cdots, N\}$) is defined as:

$$V_{structure,k} = \frac{1}{4}\lambda_{str}\left((\boldsymbol{r}_k - \boldsymbol{r}_{VL}) \cdot (\boldsymbol{r}_k - \boldsymbol{r}_{VL}) - R^2\right)^2 \tag{4}$$

where $\boldsymbol{r}_k = [x_k, y_k, z_k]^T$ and $\boldsymbol{r}_{VL} = [x_{VL}, y_{VL}, z_{VL}]^T$ denote the position vector of the k-th spacecraft and the virtual leader, respectively. $V_{structure,k}$ becomes zero only if the k-th spacecraft is placed on the sphere. Similarly, the structural potential for locating the k-th spacecraft on a (two-dimensional) circle with its radius R in the yz-plane is defined as follows:

$$V_{structure,k} = \frac{1}{4}\lambda_{str}\left[\left((y_k - y_{VL})^2 + (z_k - z_{VL})^2 - R^2\right)^2 + 2(x_k - x_{VL})^2\right] \tag{5}$$

Once those spacecraft are placed on a sphere/circle with their virtual leader located at the center, it remains to keep equidistant between the actual spacecraft to form a desired tetrahedral/polygonal shape. Every spacecraft can be considered as an electric charge for that purpose; the distances are expanded by Coulomb's law such that the objects with the same electric charge generate repulsion (Rezaee and Abdollahi, 2013). All the spacecraft are considered to possess the same charge except the virtual leader. Let $\boldsymbol{r}_{ki} = \boldsymbol{r}_k - \boldsymbol{r}_i$ $(i \neq k)$ be the relative distance between the i-th and k-th spacecraft. The repulsive potentials of the k-th spacecraft for regular polygonal and tetrahedral formations are respectively defined as Hwang (2019)

$$\begin{cases} V_{rep,k} = \lambda_{rep} q_k \sum_{i=1, i\neq k}^{N} q_i \sqrt{\frac{1}{\boldsymbol{r}_{ki} \cdot \boldsymbol{r}_{ki}}}, \\ V_{rep,k} = \lambda_{rep} q_k \sum_{i=1, i\neq k}^{N} q_i \sqrt{\left(\frac{1}{\|\boldsymbol{r}_{ki}\|} - \frac{1}{4R/\sqrt{6}}\right)\left(\frac{1}{\|\boldsymbol{r}_{ki}\|} - \frac{1}{4R/\sqrt{6}}\right)}, \end{cases} \tag{6}$$

where q_k and q_i denote the electric charges of the k-th and the i-th spacecraft, respectively, and λ_{rep} is a positive scaling factor of the repulsive potential. Note that the collision avoidance between each spacecraft can be performed by the repulsive potential with proper parameter selections.

Now the above described *structural* and *repulsive* potentials are integrated together to compose a *formation* potential as follows:

$$V_{form,k} = V_{structure,k} + V_{rep,k} + \frac{1}{2}\lambda_v \dot{\boldsymbol{r}}_k \cdot \dot{\boldsymbol{r}}_k \tag{7}$$

Here, the third term is a velocity term, which forces the velocities of spacecraft to vanish when they reach the target. The positive scaling factor λ_v may be tuned to maintain the spacecraft speed low and enable delicate maneuvers.

In practice, if obstacles can be detected in advance, it is desirable to design a reference trajectory for formation while avoiding obstacles a priori. In this research, a reference trajectory is designed without considering avoidance maneuvers. To construct a reference trajectory of a virtual leader without considering obstacles, an attractive potential ($V_{\text{attractive},VL}$) is defined as Badawy and McInnes (2008),

$$V_{attractive,VL} = \lambda_p \|\boldsymbol{r}_{VL} - \boldsymbol{r}_{VL,goal}\| + \frac{1}{2}\lambda_v \dot{\boldsymbol{r}}_{VL} \cdot \dot{\boldsymbol{r}}_{VL} \tag{8}$$

where $\boldsymbol{r}_{VL,goal}$ denotes the target point of virtual leader, $\dot{\boldsymbol{r}}_{VL}$ denotes the velocity vector of the virtual leader, and λ_p and λ_v are positive scaling factors. The potential (V_{VL}) converges to zero when the virtual leader reaches the target point and remains stationary. The total potential for formation flying ($V_{form,tot}$) then becomes

$$V_{form,tot} = V_{attractive,VL} + \sum_{k=1}^{N} V_{form,k} \tag{9}$$

The time derivative of the proposed potential ($\dot{V}_{form,tot}$) are derived as

$$\begin{aligned}\dot{V}_{form,tot} &= \dot{V}_{attractive,VL} + \sum_{k=1}^{N} \dot{V}_{form,k} \\ &= \dot{\boldsymbol{r}}_{VL} \cdot \left\{ \lambda_p \frac{(\boldsymbol{r}_{VL} - \boldsymbol{r}_{VL,goal})}{\|\boldsymbol{r}_{VL} - \boldsymbol{r}_{VL,goal}\|} - \sum_{k=1}^{N} \nabla V_{structure,k} + \lambda_v \ddot{\boldsymbol{r}}_{VL} \right\} \\ &\quad + \sum_{k=1}^{N} \left[\dot{\boldsymbol{r}}_k \cdot \left(\nabla V_{structure,k} + 2\nabla V_{rep,k} + \lambda_v \ddot{\boldsymbol{r}}_k \right) \right]\end{aligned} \tag{10}$$

Here, the time derivative of the sum of formation potential ($\sum_{k=1}^{N} \dot{V}_{form,k}$) yields $2\nabla V_{rep,k}$ as it includes $(\boldsymbol{r}_k - \boldsymbol{r}_i)$ term. The desired acceleration of the k-th spacecraft ($\ddot{\boldsymbol{r}}_{k,desired}$) can be derived such that the derivative of the total potential for formation flying becomes negative semi-definite ($\dot{V}_{form,\text{tot}} \leq 0$):

$$\ddot{\boldsymbol{r}}_{k,desired} = -\frac{1}{\lambda_v}\left(\nabla V_{structure,k} + 2\nabla V_{rep,k} + \lambda_{vk} \dot{\boldsymbol{r}}_k \right) \tag{11}$$

The desired acceleration of the virtual leader ($\ddot{\boldsymbol{r}}_{VL,desired}$) can be derived as

$$\ddot{\boldsymbol{r}}_{VL,desired} = -\frac{1}{\lambda_v}\left(\lambda_p \frac{(\boldsymbol{r}_{VL} - \boldsymbol{r}_{VL,goal})}{\|\boldsymbol{r}_{VL} - \boldsymbol{r}_{VL,goal}\|} - \sum_{k=1}^{N} \nabla V_{structure,k} + \lambda_{vk,VL} \dot{\boldsymbol{r}}_{VL} \right) \tag{12}$$

where λ_{vk} and $\lambda_{vk,VL}$ are positive parameters that slow down the speed as they become larger.

The control law of the k-th spacecraft ($\boldsymbol{u}_k$) for formation flying on a circle and in a regular tetrahedron is given as follows:

$$\boldsymbol{u}_k = \ddot{\boldsymbol{r}}_{k,desired} - f_k(\boldsymbol{r}_k, \dot{\boldsymbol{r}}_k) \tag{13}$$

We cite Hwang (2019) for detailed derivation of the above control law and its stability analysis.

4. Rotational potential for collision avoidance

The obstacle avoidance of spacecraft in formation can be also achieved by implementing an appropriate potential. However, the currently used potential for obstacle avoidance in literature often leads to undesired local minima on its own; if an obstacle is located symmetrically along the trajectory of spacecraft, the repulsive force to avoid obstacles and the attractive force to reach the target combine to generate an undesired equilibrium, which leads to cancelling out both the attractive and repulsive forces to make the spacecraft stuck (Warren, 1989).

This research directly addresses this issue of undesired local minimum by introducing a newly defined *rotational potential*. An appropriate rotational potential is designed for a spacecraft to detour obstacles through behavioral approach. Unlike the conventional avoidance potential, our proposed rotation potential does not simply operate in the opposite direction to the obstacle, but works actively to avoid the obstacles. We first derive an appropriate rotational potential for collision avoidance based on the associated *rotational force* function.

4.1. Rotational force function in 2-Dimensional space

Consider, for example, a rectangular obstacle whose centre is located at $[x_0, y_0]^T$ and whose sides parallel to the x-axis and y-axis are $2a$ and 2 b, respectively, in the xy-plane. As can be seen in Fig. 2, the equation for ellipse completely covering all the vertices of the rectangle can be represented as

$$\frac{(x - x_0)^2}{2a^2} + \frac{(y - y_0)^2}{2b^2} = 1 \tag{14}$$

The velocity vector of the k-th spacecraft ($\dot{\boldsymbol{r}}_k$) is set up as follows such that it moves clockwise and tangent to the ellipse:

$$\begin{aligned}\dot{\boldsymbol{r}}_k &= \dot{x}_k \hat{x} + \dot{y}_k \hat{y} \\ \dot{x}_k &= \frac{a}{b}(y_k - y_0) \\ \dot{y}_k &= -\frac{b}{a}(x_k - y_0)\end{aligned} \tag{15}$$

Rezaee and Abdollahi (2013) have shown that the artificial force vector ($\boldsymbol{f}_{rot}$) that actuates the k-th spacecraft to follow Eq. (15) can be derived as follows:

$$\boldsymbol{f}_{rot} = f_{rot,x} \hat{x} + f_{rot,y} \hat{y}$$

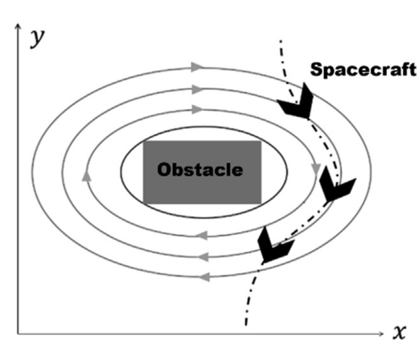

Fig. 2. Rotational force affecting spacecraft trajectory near obstacle.

$$f_{rot,x} = \frac{a}{b}(y_k - y_0)$$

$$f_{rot,y} = -\frac{b}{a}(x_k - y_0) \tag{16}$$

Maneuvering the spacecraft tangent to the ellipse does not cancel out the net force in a straight line, and thus avoid being stuck at an undesired local minimum. Based on Eq. (16), the rotational force function ($\boldsymbol{F}_{rot}$) in two-dimensional space can be designed as follows:

$$\boldsymbol{F}_{rot} = \lambda_r \frac{\boldsymbol{f}_{rot}}{\|\boldsymbol{f}_{rot}\|} exp(-\lambda_{rot} d_k) \tag{17}$$

Here d_k denotes the relative distance between the k-th spacecraft and obstacle. The design parameter λ_{rot} determines how steeply the force increases depending on the relative distance; if λ_{rot} becomes higher, the rate of increase of force function becomes higher as the spacecraft approaches the obstacle. λ_r is a scaling factor of the rotational force function. In summary, the force vector in Eq. (17) determines the direction of the rotational force function, and λ_r determines the magnitude of the function depending on the relative distance.

4.2. Rotational potential for 3-Dimensional space

Rezaee and Abdollahi (2013) have first introduced the above rotational force function that enables a spacecraft to avoid obstacles in *2-dimensional* space. As this research considers formation flying in 3-dimensional space, we now extend the rotational force function into *3-dimensional* space. This section is dedicated to *newly* deriving a *rotational potential* (not just a rotational force function) in 3-dimensional space and integrating it into the APF derived in Section 3. This allows us to design a control law for spacecraft formation flying with obstacle avoidance by a *single* scalar function and to analyse stability as well. The overall process can be summarized as follows:

STEP 1. Define a 3-dimensional local coordinate frame centred on the obstacle.
STEP 2. Select a plane including a collision-free path in the local frame.
STEP 3. Derive a rotational force function in the plane in **STEP 2**.
STEP 4. Derive a *rotational potential* from the rotational force function in **STEP 3**.

In order to extend the 2-dimensional (2-D) rotational force function into 3-dimensional (3-D) one, a 3-D coordinate frame whose origin is centred at the obstacle is first defined. Then, the 2-D plane on which a spacecraft detours the obstacle on a shortest path is chosen as the plane in which the 2-D rotational force function is derived. Once the 2-D rotational force function is derived, it is converted into *3-D rotational potential.*

STEP 1. Define a 3-dimensional local coordinate frame centred at the obstacle

Consider a rectangular reference frame $\boldsymbol{C} : \{\hat{\boldsymbol{x}}, \hat{\boldsymbol{y}}, \hat{\boldsymbol{z}}\}$ with its origin at O in Fig. 3. Let $\boldsymbol{r}_{obs} = \left(r_{obs,x}, r_{obs,y}, r_{obs,z}\right)$ be the position vector of an obstacle, $\boldsymbol{r} = \left(r_x, r_y, r_z\right)$ be the position vector of a spacecraft and $\boldsymbol{r}_G = \left(r_{G,x}, r_{G,y}, r_{G,z}\right)$ be the position vector of target point. A local 3-D coordinate frame $\boldsymbol{B} : \left\{\hat{\boldsymbol{h}}, \hat{\boldsymbol{n}}, \hat{\boldsymbol{i}}\right\}$, whose origin is located at the center of the obstacle, is defined (Fig. 3). The unit vector $\hat{\boldsymbol{h}}$ directs from the obstacle to the spacecraft, the direction of $\hat{\boldsymbol{n}}$ comes from the cross product of $\hat{\boldsymbol{h}}$ and the target vector from the origin O', and the direction of $\hat{\boldsymbol{i}}$ completes the right-hand coordinate system.

$$\boldsymbol{B} : \left\{\hat{\boldsymbol{h}}, \hat{\boldsymbol{n}}, \hat{\boldsymbol{i}}\right\},\ \hat{\boldsymbol{h}} = \frac{\boldsymbol{r} - \boldsymbol{r}_{obs}}{|\boldsymbol{r} - \boldsymbol{r}_{obs}|},\ \hat{\boldsymbol{n}} = \frac{(\boldsymbol{r}_G - \boldsymbol{r}_{obs}) \times \hat{\boldsymbol{h}}}{\left|(\boldsymbol{r}_G - \boldsymbol{r}_{obs}) \times \hat{\boldsymbol{h}}\right|},$$
$$\hat{\boldsymbol{i}} = \frac{\hat{\boldsymbol{h}} \times \hat{\boldsymbol{n}}}{\left|\hat{\boldsymbol{h}} \times \hat{\boldsymbol{n}}\right|} \tag{18}$$

If the transformation matrix $\boldsymbol{T}$ from the reference frame ($\boldsymbol{C}$) to the local frame ($\boldsymbol{B}$) is defined, then the position vector of spacecraft in the local frame (${}^{B}r$) is expressed as

$${}^{\boldsymbol{B}}\boldsymbol{r} = \boldsymbol{T} \cdot (\boldsymbol{r} - \boldsymbol{r}_{obs}) \tag{19}$$

STEP 2. Select a plane including a collision-free path in the local frame

Suppose that the rectangular obstacle located at $\boldsymbol{r}_{obs} = \left(r_{obs,x}, r_{obs,y}, r_{obs,z}\right)$ has the sides of $(2a, 2b, 2c)$ along each axis in frame $\boldsymbol{C}$. Similar to Eq. (14), an ellipsoid with the smallest volume enclosing the rectangle can be expressed as

$$\frac{\left(x - r_{obs,x}\right)^2}{2a^2} + \frac{\left(y - r_{obs,y}\right)^2}{2b^2} + \frac{\left(z - r_{obs,z}\right)^2}{2c^2} = 1 \tag{20}$$

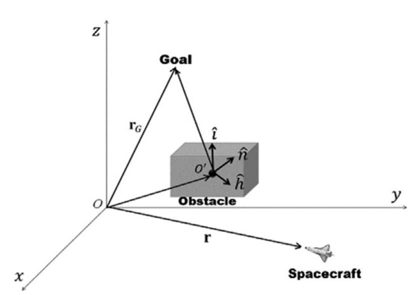

Fig. 3. Reference frame $\boldsymbol{C}$ and local frame $\boldsymbol{B}$.

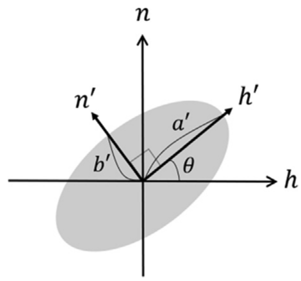

Fig. 4. (1) Rotated ellipse with a semi-major axis $\boldsymbol{a}$ and a semi-minor axis $\boldsymbol{b}'$, (2) Rotated h'&n'-axes by an angle $\boldsymbol{\theta}$ from h&n-axes.

As an arbitrary position $[x, y, z]^T$ in frame $\boldsymbol{C}$ can be represented by a vector $[h, n, i]^T$ in frame $\boldsymbol{B}$ through the following transformation

$$\begin{bmatrix} x - r_{obs,x} \\ y - r_{obs,y} \\ z - r_{obs,z} \end{bmatrix} = \boldsymbol{T}^{-1} {}^{B}\begin{bmatrix} h \\ n \\ i \end{bmatrix} = {}^{B}\begin{bmatrix} \alpha_1 & \alpha_2 & \alpha_3 \\ \alpha_4 & \alpha_5 & \alpha_6 \\ \alpha_7 & \alpha_8 & \alpha_9 \end{bmatrix} \begin{bmatrix} h \\ n \\ i \end{bmatrix}, \tag{21}$$

The obstacle ellipsoid can be expressed in frame $\boldsymbol{B}$ as follows:

$$\frac{(\alpha_1 h + \alpha_2 n + \alpha_3 i)^2}{2a^2} + \frac{(\alpha_4 h + \alpha_5 n + \alpha_6 i)^2}{2b^2} + \frac{(\alpha_7 h + \alpha_8 n + \alpha_9 i)^2}{2c^2} = 1 \tag{22}$$

Now, a 2-D plane, on which the rotational force function is to be derived, needs to be selected. For that purpose, a plane of the ellipse with lower eccentricity is specifically selected between the two ellipses created by the intersection of the obstacle ellipsoid and each of the hn-plane and hi-plane. Note that only the plane containing the h-axis is available since the spacecraft is on the h-axis. We cite Hwang (2019) for the detailed derivation.

STEP 3. Derive a rotational force function in the plane in STEP 2

Suppose that a plane created by the intersection of obstacle ellipsoid and the hn-plane is selected to construct the rotational force function. As the equation for hn-plane is expressed as $i = 0$, the following equations needs to be solved simultaneously:

$$\left\{ \frac{(\alpha_1 h + \alpha_2 n + \alpha_3 i)^2}{2a^2} + \frac{(\alpha_4 h + \alpha_5 n + \alpha_6 i)^2}{2b^2} + \frac{(\alpha_7 h + \alpha_8 n + \alpha_9 i)^2}{2c^2} = 1 i = 0 \cdot, \right. \tag{23}$$

which leads to

$$Ah^2 + Cn^2 + Bhn = 1$$

$$\text{where } A = \left(\frac{\alpha_1^2}{2a^2} + \frac{\alpha_4^2}{2b^2} + \frac{\alpha_7^2}{2c^2}\right),\ B = 2\left(\frac{\alpha_1\alpha_2}{2a^2} + \frac{\alpha_4\alpha_5}{2b^2} + \frac{\alpha_7\alpha_8}{2c^2}\right),\ C = \left(\frac{\alpha_2^2}{2a^2} + \frac{\alpha_5^2}{2b^2} + \frac{\alpha_8^2}{2c^2}\right) \tag{24}$$

Let h'-axis and n'-axis be the counterclockwise rotation from the h-axis and the n-axis, respectively, by the angle θ (Fig. 4). Then, h' and n' can be obtained as follows:

$$h' = hcos\theta + nsin\theta,\ n' = -hsin\theta + ncos\theta \tag{25}$$

Rearranging Eq. (25) for h and n and applying to Eq. (24) yields

$$A'h'^2 + C'n'^2 + B'h'n' = 1 \tag{26}$$

where

$$A' = Acos^2\theta + Bsin\theta cos\theta + Csin^2\theta$$
$$C' = Asin^2\theta - Bsin\theta cos\theta + Ccos^2\theta$$
$$B' = 2(C - A)sin\theta cos\theta + B\left(cos^2\theta - sin^2\theta\right) \tag{27}$$

The value of θ to make $h'n'$-term become zero $\left(B' = 0\right)$ is:

$$\theta = \frac{1}{2}tan^{-1}\left(\frac{B}{A - C}\right),\ \theta \in \left(-\frac{\pi}{2}, \frac{\pi}{2}\right) \tag{28}$$

Eq. (28) is not defined when $A - C = 0$, as the intersection becomes a circle, i.e., $\theta = \pm\pi/4$. Similarly in the case of non-tilting ellipse, i.e., Eq. (14), the semi-major axis (a') and semi-minor axis (b') of the ellipse are obtained as follows:

$$a' = \sqrt{\frac{1}{A'}},\ b' = \sqrt{\frac{1}{C'}} \tag{29}$$

With the help of Eq. (25), the elliptic equation that is rotated by θ ($\frac{h'^2}{a'^2} + \frac{n'^2}{b'^2} = 1$) is expressed in the hn-plane as

$$\frac{(hcos\theta + nsin\theta)^2}{a'^2} + \frac{(hsin\theta - ncos\theta)^2}{b'^2} = 1 \tag{30}$$

In the way the required velocity vector in Eq. (15) is obtained from Eq. (14), Eq. (30) similarly leads to the following simultaneous equations of the required velocity vector of the k-th spacecraft:

$$\begin{cases} \dot{h}_k cos\theta + \dot{n}_k sin\theta = \frac{a'}{b'}(h_k sin\theta - n_k cos\theta), \\ \dot{h}_k sin\theta - \dot{n}_k cos\theta = -\frac{b'}{a'}(h_k cos\theta + n_k sin\theta). \end{cases} \tag{31}$$

By solving Eq. (31), the required velocity vector $(\dot{h}_k, \dot{n}_k)$ of the k-th spacecraft to move clockwise and tangent to the ellipse is derived as follows:

$$\begin{cases} \dot{h}_k = \left(\frac{a'}{b'} + \frac{b'}{a'}\right)cos\theta sin\theta h_k + \left(\frac{b'}{a'}sin^2\theta - \frac{a'}{b'}cos^2\theta\right)n_k, \\ \dot{n}_k = \left(\frac{a'}{b'}sin^2\theta + \frac{b'}{a'}cos^2\theta\right)h_k + \left(\frac{b'}{a'} - \frac{a'}{b'}\right)cos\theta sin\theta n_k. \end{cases} \tag{32}$$

The artificial force vector ($\boldsymbol{f}_{rot,hn} = f_{rot,h}\hat{\boldsymbol{h}} + f_{rot,n}\hat{\boldsymbol{n}}$) of the k-th spacecraft for avoidance maneuver in the hn-plane can be derived to follow Eq. (32) in the same way that Eq. (16) is derived to follow Eq. (15):

$$\begin{cases} f_{rot,h} = c_1 h_k + c_2 n_k, \\ f_{rot,n} = c_3 h_k + c_4 n_k, \end{cases} \tag{33}$$

$$c_1 = \left(\frac{a'}{b'} + \frac{b'}{a'}\right)\cos\theta\sin\theta,\ c_3 = \left(\frac{a'}{b'}\sin^2\theta + \frac{b'}{a'}\cos^2\theta\right),\ c_2 = \left(\frac{b'}{a'}\sin^2\theta - \frac{a'}{b'}\cos^2\theta\right),\ c_4 = \left(\frac{b'}{a'} - \frac{a'}{b'}\right)\cos\theta\sin\theta$$

Eq. (33) is used to define the rotational force function ($\boldsymbol{F}_{rot,hn}$) of the k-th spacecraft in the hn-plane as

$$\boldsymbol{F}_{rot,hn} = \lambda_r \frac{\boldsymbol{f}_{rot,hn}}{\|\boldsymbol{f}_{rot,hn}\|} exp(-\lambda_{rot} d_k) \quad (34)$$

where d_k denotes the relative distance between the k-th spacecraft and the obstacle and will be rigorously defined in the subsequent STEP 4. The parameter λ_{rot} determines how steeply the force increases as the relative distance changes. The parameter λ_r is a scaling factor of the rotational force function. As the spacecraft moves away from the obstacle, the force becomes exponentially smaller.

STEP 4. Derive a rotational potential from STEP 3

It now remains to derive a *rotational potential* associated with the rotational force function in Eq. (34). Note that the k-th spacecraft is located on the positive h-axis and the rotational force function is recalculated at each moment the spacecraft needs to avoid obstacles. Thus, the k-th spacecraft is positioned at $[h_k, 0, 0]^T$, $h_k > 0$ in the local coordinates. With $n_k = 0$, the rotational force function becomes

$$\begin{cases} F_{rot,h} = \lambda_r \frac{c_1}{\sqrt{{c_1}^2 + {c_3}^2}} exp(-\lambda_{rot} d_k), \\ F_{rot,n} = \lambda_r \frac{c_3}{\sqrt{{c_1}^2 + {c_3}^2}} exp(-\lambda_{rot} d_k), \end{cases} \quad (35)$$

where d_k denotes the distance between the k-th spacecraft and the obstacle ellipse:

$$d_k = h_k - \frac{1}{\sqrt{A}} \quad (36)$$

In order to deriving the rotational potential, the well-known theorem is used: *the negative gradient of a potential V is the associated (artificial) force F*, i.e., $\boldsymbol{F} = -\nabla V$ (Badawy and McInnes, 2008). Applying this theorem to Eq. (35) leads to

$$\boldsymbol{F}_{rot,hn} = -\nabla^* V_{rot,k} \quad (37)$$

$$V^{tmp}_{rot,k} = -\int F_{rot,h} dh_k - \int F_{rot,n} dn_k \quad (38)$$

Eq. (38) is defined as the temporary rotational potential $V^{tmp}_{rot,k}$, as it does not converge to zero when the spacecraft reaches the desired target. A function $A(\mathbf{r})$ is multiplied to the temporary rotational potential such that it vanishes at the target:

Definition.. *Let the angle θ be the angle between h-axis and h'-axis. Let $d = h - \frac{1}{\sqrt{A}}$ and $D = h - \frac{1}{\sqrt{C}}$. The rotational potential (V_{rot}) is defined as*

$$\begin{cases} V_{rot} = \lambda_r A(\boldsymbol{r}) \left(\frac{c_1}{\lambda_{rot}} - c_3 n\right) \frac{exp(-\lambda_{rot} d)}{\sqrt{c_1^2 + c_3^2}} & if\ sin2\theta \geq 0, \\ V_{rot} = \lambda_r A(\boldsymbol{r}) \left(\frac{c_5}{\lambda_{rot}} - c_6 n\right) \frac{exp(-\lambda_{rot} D)}{\sqrt{c_5^2 + c_6^2}} & if\ sin2\theta < 0, \end{cases} \quad (39)$$

$$A(\mathbf{r}) = 1 - \exp\left(-\frac{1}{\sigma}\left(\left(\boldsymbol{r} - \boldsymbol{r}_{VL,goal}\right)\cdot\left(\boldsymbol{r} - \boldsymbol{r}_{VL,goal}\right) - R^2\right)^2\right),\ c_1 = \frac{1}{2}\left(\frac{a'}{b'} + \frac{b'}{a'}\right)\sin 2\theta,\ c_3 = \left(\frac{a'}{b'}\sin^2\theta + \frac{b'}{a'}\cos^2\theta\right),\ c_5 = \frac{1}{2}\left(\frac{a'}{b'} + \frac{b'}{a'}\right)\sin 2\left(\theta - \frac{\pi}{2}\right),\ c_6 = \frac{b'}{a'}\sin^2\left(\theta - \frac{\pi}{2}\right) + \frac{a'}{b'}\cos^2\left(\theta - \frac{\pi}{2}\right)$$

Note that the above rotational force function and its associated potential are defined in the local hn-plane. The rotational force function can be transformed into the reference frame $\boldsymbol{C}$ through transformation $\boldsymbol{T}^{-1}$ in Eq. (21):

$$\boldsymbol{F}_{rot} = \boldsymbol{T}^{-1} \cdot [\boldsymbol{F}_{rot,hn}, 0]^T \quad (40)$$

So far, the states of spacecraft have been used to define the 3-D local coordinate frame, in which the rotational force function and its associated rotational potential have been constructed and calculated at each moment the spacecraft needs to maneuver for collision avoidance. With the potential defined as such, the control law for formation flying with collision avoidance is derived in the following Section 4.3.

4.3. Lyapunov-based continuous control law

With the structural & repulsive potentials for maintaining the desired formation and the rotational potential for collision avoidance integrated into one synthesized function, a continuous control law can be derived for a group of spacecraft in formation. The equations of motion for the k-th spacecraft subject to HCW dynamics is given as

$$\ddot{\boldsymbol{r}}_k = f_k(\boldsymbol{r}_k, \dot{\boldsymbol{r}}_k) + \boldsymbol{u}_k \quad (41)$$

where $\boldsymbol{r}_k = [x_k, y_k, z_k]^T, \dot{\boldsymbol{r}}_k = [\dot{x}_k, \dot{y}_k, \dot{z}_k]^T, f_k(\boldsymbol{r}_k, \dot{\boldsymbol{r}}_k) = \left[2w_0\dot{y} + 3w_0^2 x, -2w_0\dot{x}, -w_0^2 z\right]^T, \boldsymbol{u}_k = \left[u_{k,x}, u_{k,y}, u_{k,z}\right]^T$.

Consider, for example, relative motion of (active) spacecraft with respect to a reference (passive) spacecraft in a circular orbit at an altitude $h\ km$. The angular velocity of the reference spacecraft is $w_0 = \sqrt{(R_E + h)}$ where R_E and M_E are the radius and mass of the Earth, respectively. In order to maintain multiple spacecraft in the formation of regular polygon/tetrahedron while avoiding collision, the potential of the k-th spacecraft ($V_{total,k}$) is constructed as the sum of the formation potential ($V_{form,k}$) and the rotational potential ($V_{rot,k}$):

$$V_{total,k} = V_{form,k} + V_{rot,k} \tag{42}$$

Then, the total potential for all spacecraft can be written as follows:

$$V_{total} = V_{total,VL} + \sum_{k=1}^{N} V_{total,k}. \tag{43}$$

The desired control acceleration of the k-th spacecraft is designed as

$$\ddot{\mathbf{r}}_{k,desired} = -\frac{1}{\lambda_v}\Big(\nabla V_{structure,k} + 2\nabla V_{rep,k} + V_{rot,k}^{tmp}\nabla A_k + A_k \boldsymbol{T}^{-1}\cdot\nabla^* V_{rot,k}^{tmp} + \lambda_{vk}\ddot{\boldsymbol{r}}_k\Big) \tag{44}$$

where $A_k = A(\mathbf{r}_k)$. Note that $\boldsymbol{F}_{rot,hn} = -\nabla^* V_{rot,k}$ and $\boldsymbol{F}_{rot} = \boldsymbol{T}^{-1}\cdot\boldsymbol{F}_{rot,hn}$. With Eq. (44), the time derivative of the total potential becomes negative semi-definite:

$$\dot{V}_{total} = -\sum_{k=1}^{N}\lambda_{vk}\dot{\boldsymbol{r}}_k\cdot\dot{\boldsymbol{r}}_k - \lambda_{vk,VL}\dot{\boldsymbol{r}}_{VL}\cdot\dot{\boldsymbol{r}}_{VL} \le 0 \tag{45}$$

The continuous control law $\boldsymbol{u}_k$ for the k-th spacecraft is obtained from Eq. (44) as

$$\boldsymbol{u}_k = -\left(\nabla V_{structure,k} + \nabla V_{rep,k} + V_{rot,k}^{tmp}\nabla A_k + A_k\boldsymbol{T}^{-1}\cdot\nabla^* V_{rot,k} + \frac{\lambda_{vk}}{\lambda_v}\dot{\boldsymbol{r}}_k\right) - f_k(\boldsymbol{r}_k,\dot{\boldsymbol{r}}_k) \tag{46}$$

where $f_k(\boldsymbol{r}_k,\dot{\boldsymbol{r}}_k)$ denotes HCW dynamics in Eq. (41).

To ensure collision avoidance with obstacles, it may be considered to add the following avoidance potential to the rotational potential:

$$V_{avoid,k} = \lambda_{avoid}\frac{exp(-\lambda_o d_k)}{d_k} \tag{47}$$

where d_k denotes the Euclidean distance between the spacecraft and obstacle surface, and λ_{avoid} and λ_o are scaling factors. If d_k approaches zero, an exponential function of $V_{avoid,k}$ becomes exponentially large, which ensures that the spacecraft do not collide with obstacles. The example of Case 3 in Section 5 considers the control law including this *auxiliary* term for obstacle avoidance, but Cases 1 and 2 do not consider this term for collision avoidance and use only the rotational potential function to demonstrate that the spacecraft can avoid an obstacle without using the avoidance potential function. However, the avoidance potential should be added to ensure collision-free maneuvers in actual missions.

5. Numerical simulations and analysis

The proposed control law is validated through three distinctive numerical simulations. The positions and velocities of all the spacecraft and obstacles are assumed to be known. With a desktop computer with Intel® Core™ i7-7700 K CPU @4.20 GHz, the computation time for the control law is less than 0.02 s in each step.

Case 1. Mitigation of convergence to an undesired local minimum

In order to focus on demonstrating the mitigation of convergence to an undesired local minimum, consider a simple example of *single spacecraft without dynamics*: a spacecraft is initially located at $\boldsymbol{r}_0 = [-5,0,0]^T m$ in the inertial frame $\boldsymbol{I}:\{\hat{\boldsymbol{x}},\hat{\boldsymbol{y}},\hat{\boldsymbol{z}}\}$; the control objective is to transfer the spacecraft to the target point $\boldsymbol{r}_{goal} = [-140,0,0]^{\mathrm{T}} m$ while avoiding a rectangular parallelepiped located at $\boldsymbol{r}_{obs} = [-70,0,0]^{\mathrm{T}} m$ with the dimension of $40\times 20\times 20m$; note that the center of the obstacle ($\boldsymbol{r}_{obs}$), the initial position of the spacecraft ($\boldsymbol{r}_0$), and the target point ($\boldsymbol{r}_{goal}$) are aligned on a straight line. The performance of our proposed control law (Method A) is compared with that of Method B based on APF (Badawy and McInnes, 2008) which has been also developed for mitigating the issue of undesired local minima.

With the total potential of the spacecraft defined as

$$\begin{aligned} V_{tot} &= V_{att} + \frac{1}{2}\lambda_v\dot{\boldsymbol{r}}\cdot\dot{\boldsymbol{r}} + V_{avoid} \\ &= \lambda_p\|\boldsymbol{r}-\boldsymbol{r}_{goal}\| + \frac{1}{2}\lambda_v\dot{\boldsymbol{r}}\cdot\dot{\boldsymbol{r}} + \lambda_{avoid}\frac{exp(-\lambda_o K)}{K} \end{aligned} \tag{48}$$

where K denotes the radial separation distance between spacecraft and the obstacle's superquadric surface. The associated feedback control $\boldsymbol{u}$ is designed such that the time derivative of the total potential becomes negative semi-definite:

$$\boldsymbol{u} = -\left(\frac{\lambda_p}{\lambda_v}\frac{(\boldsymbol{r}-\boldsymbol{r}_{goal})}{\|\boldsymbol{r}-\boldsymbol{r}_{goal}\|} + \frac{\lambda_{vk}}{\lambda_v}\dot{\boldsymbol{r}} + \nabla V_{avoid}\right) \tag{49}$$

Scaling factors and design parameters in Methods A & B are set as $\lambda_p = 0.1$, $\lambda_v = 1$, $\lambda_{vk} = 7, \lambda_{rot} = 0.3$, $\lambda_r = 2, \lambda_{avoid} = 2$, and $\lambda_o = 40$. Fig. 5 shows the trajectories of the spacecraft for 1600 sec by both methods. The solid and dashed lines represent the resultant trajectories by Methods A & B, respectively. The grey rectangular parallelepiped and the grey star represent the obstacle and the target point, respectively. The spacecraft is initially located at Δ, and transferred to $\circ$ at the final time. While Method A safely drives the spacecraft to the target point without collision, Method B leads the spacecraft to being stuck in front of the obstacle, i.e., at an undesired local minimum. Even if the avoidance potential can be designed more rigorously with superquadrics, Method B cannot lead the spacecraft to detour since both the attractive and repulsive forces act in the opposite direction on a straight line; it simply repeats moving back and forth in that straight line by the interaction of attractive and repulsive forces, and is ultimately trapped.

Case 2. Effects of rotational potential for 3-dimensional formation flying with collision avoidance

Chang et al. (2016) extended the 2-dimensional rotational *force function* proposed by Rezaee and Abdollahi (2013) into 3-dimensional one, and developed their collision avoidance algorithm to resolve the local minimum

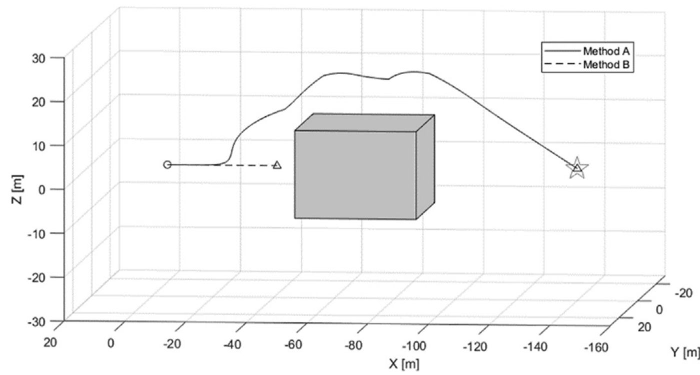

Fig. 5. Spacecraft trajectories by Methods A (solid line) & B (dashed line); initial position (Δ), final position (○), target point (grey star), and obstacle (grey face).

issue. The overall approach was applied to the collision avoidance maneuvers for a group of unmanned aerial vehicles (UAVs) in formation. In this example, the Scenario 3 of Chang et al. (2016), which is an example for *UAV* formation flying, is reformulated as a collision avoidance problem for a group of *spacecraft* in formation. As a virtual leader is considered as a leader spacecraft which must also avoid collisions in this example, collision avoidance term is added to the control law of the leader in the Eq. (12).

Consider a group of four (active) spacecraft $(\boldsymbol{r}_1, \boldsymbol{r}_2, \boldsymbol{r}_3, \boldsymbol{r}_4)$ to move toward a target point while avoiding an obstacle. They form a square on a circle with its radius $R = 2m$ in the yz-plane, and are initially located at $\boldsymbol{r}_{1,0} = [0.5, 1, 2.5]^T m$, $\boldsymbol{r}_{2,0} = [3.5, 3.5, 7]^T m$, $\boldsymbol{r}_{3,0} = [2, -1, 6.5]^T m$, and $\boldsymbol{r}_{4,0} = [2, 3, 6.5]^T m$. A (active) leader spacecraft is initially located at the center of the circle, i.e., at $\boldsymbol{r}_{VL,0} = [1, 1, 5.5]^T m$, and is required to reach the target point at $\boldsymbol{r}_{VL,goal} = [30, 30, 15]^{\mathrm{T}} m$ while avoiding the obstacle. The obstacle is a stationary $2 \times 3 \times 3m$ rectangular parallelepiped centered at $\boldsymbol{r}_{obs} = [20, 20, 10]^T m$. All the spacecraft are subject to HCW dynamics described in Section 2, and the radius of nominal orbit is $(R_E + 408)km$. Minimum allowable distance between the spacecraft and the obstacle is assigned as $3m$. Four spacecraft are required to maintain the square formation. During maneuvers, the minimum distance between the virtual leader and each spacecraft is not smaller than $2\sqrt{2}$ $2.83m$, and the minimum distance between each spacecraft is not smaller than $2m$.

Based on the above formulation, the performances of our proposed algorithm (Method C) and Chang et al.'s algorithm (Method D) are compared with each other. In Chang et al., the original condition to activate collision avoidance maneuver was $R < (\boldsymbol{r}_k - \boldsymbol{r}_{obs})$, but it is modified into $(\boldsymbol{r}_k - \boldsymbol{r}_{obs}) < 11$, as it hardly avoids collision. Both methods use the same attractive and formation potential for formation flying.

Figs. 6 and 7 show the trajectories of spacecraft and the relative distance between spacecraft and the obstacle, respectively. It can be seen that our proposed Method C initiates maneuvering to rotate the spacecraft slightly around the obstacle by the effect of rotational potential when the distance to the obstacle is farther than $3m$. Our trajectory in Fig. 6 shows gradually avoiding trajectory, as the rotational potential is applied without constraints on the relative distance from obstacles. On the other hand, Chang et al.'s Method D starts collision avoidance maneu-

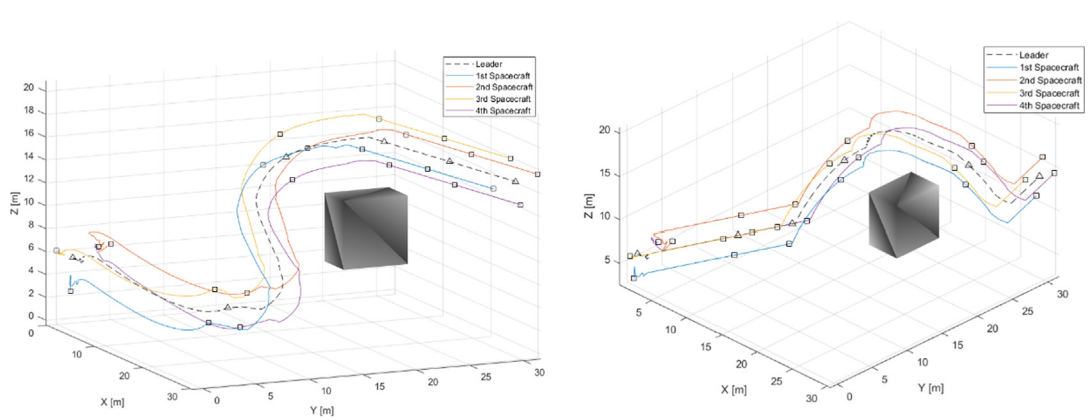

Fig. 6. Trajectories of leader and four followers with leader (Δ) and four following spacecraft (□) at t = 0, 200, 350, 500, 1000 and 3000 sec: our proposed approach (Method C; left) and Chang et al.'s approach (Method D; right).

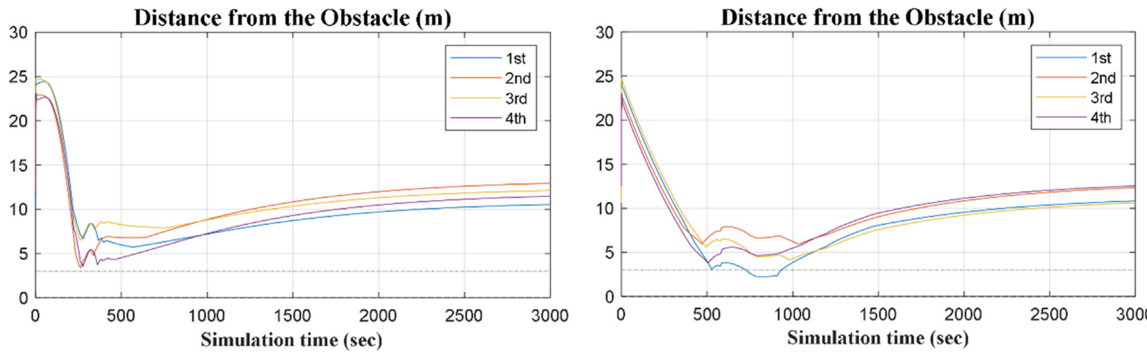

Fig. 7. Minimum distance between four spacecraft and obstacle surface: our proposed approach (Method C; left) and Chang et al.'s approach (Method D; right).

ver when the distance between the spacecraft and obstacle becomes smaller than $11m$ by the assigned activation condition. While Table 1 shows that both Methods spend similar computation time and control efforts, the right-hand side of Fig. 7 shows one of the spacecraft pass the forbidden region in Chang et al.'s Method D, which might be caused by parameter tuning or different formulation.

In addition, Case 2 was implemented using Method C for the dynamic equation with J_2 perturbation, one of the most dominant perturbations near the Earth. The resultant linearized dynamic equations of relative motion of the deputy spacecraft were given in Eq. (50) (Roberts and Roberts, 2004).

$$\ddot{x} = 2w_0 c\dot{y} + \left(5c^2 - 2\right)w_0^2 x$$
$$\ddot{y} = -2w_0\dot{x}$$
$$\ddot{z} = -\left(3c^2 - 2\right)w_0^2 z \quad (50)$$

where $c = \sqrt{1+s}$ and $s = \left(3J_2R_E^2/8r^2\right)(1 + 3cos2i)$. Here, J_2 is the second zonal gravitational coefficient according to JGM-2 model with a value of $1.082626925638815 \times 10$–3 and i is the inclination of circular chief orbit, say, 51.6° (Djojodihardj, 2014).

Since the last term in Eq. (46) offsets the effect of dynamics in the control law, Fig. 8 shows that the trajectory and distances from the obstacle do not change substantially even with the effect of J_2 perturbations. Though, the difference can be observed in control efforts which increase by about 1.78 times, as given in Table 2.

Case 3. Formation reconfiguration while avoiding collision

This example is inspired by space interferometry missions. Consider a scenario that a group of five spacecraft form/maintain a regular pentagon for a virtual telescope mission while avoiding an obstacle, one of them is broken unexpectedly, and the remaining four of them are required to *autonomously* reconfigure to form/maintain a square to continue the virtual telescope mission. Five (active) spacecraft ($\mathbf{r}_1, \mathbf{r}_2, \mathbf{r}_3, \mathbf{r}_4, \mathbf{r}_5$) initially form a regular pentagon on a circle with its radius $R = 6m$, and a virtual leader is centered on the circle in the yz-plane. The obstacle is given as a $6 \times 12 \times 6m$ rectangular parallelepiped. The control objective is to transfer those spacecraft while avoiding the obstacle farther than 5 m away from its surface. The five spacecraft are initially at rest at $\mathbf{r}_{1,0} = [2, 2, 3]^T m$, $\mathbf{r}_{2,0} = [5, 5, 3]^T m$, $\mathbf{r}_{3,0} = [4, 4, 3]^T m$, $\mathbf{r}_{4,0} = [5, 1, -3]^T m$, and $\mathbf{r}_{5,0} = [2, 4, -3]^T m$. The initial position of the (passive) virtual leader is given as $\mathbf{r}_{VL,0} = [3, -5, 0]^T m$, and the target point of the virtual leader is set as $\mathbf{r}_{VL,goal} = [-150, 0, 0]^T m$. The center of a stationary obstacle is set as $\mathbf{r}_{obs} = [-70, -3, -3]^T m$. All the spacecraft are subject to HCW dynamics described in Section 2, and the radius of nominal orbit is $(R_E + 408)km$.

Fig. 9 shows the trajectories of five satellites (□) around the virtual leader (Δ) at 150 sec, 300 sec, 450 sec,619 sec, 670 sec, 800 sec, 1000 sec, 1400 sec, 2000 sec, and 5000 sec. Although the virtual leader was not controlled to avoid collision, the gradient of structural potential term in the Eq. (12) works for avoiding collision. Fig. 10 shows the minimum distances between the spacecraft and the obstacle surface. Both figures show that the five spacecraft avoid the obstacle farther than $5.8m$ until 620 sec. Fig. 11 shows the distances between each of five satellites and the virtual leader. The relative distances between five spacecraft in formation are given in Fig. 12, where a dashed line represents the required relative distance between the spacecraft in pentagon before 900 sec and square formation after

Table 1
Comparison of computation time and cost between Method C and Method D.

Method	Our Proposed Method C	Chang et al.'s Method D
Computation Time (sec)	1687.0	1914.8
Control Effort $\sqrt{\int u \cdot u^T dt}$ (m/sec)	(1st) 16.4294 (2nd) 14.0812 (3rd) 11.1174 (4th) 6.3174	(1st) 17.0050 (2nd) 14.7710 (3rd) 11.9498 (4th) 7.5793

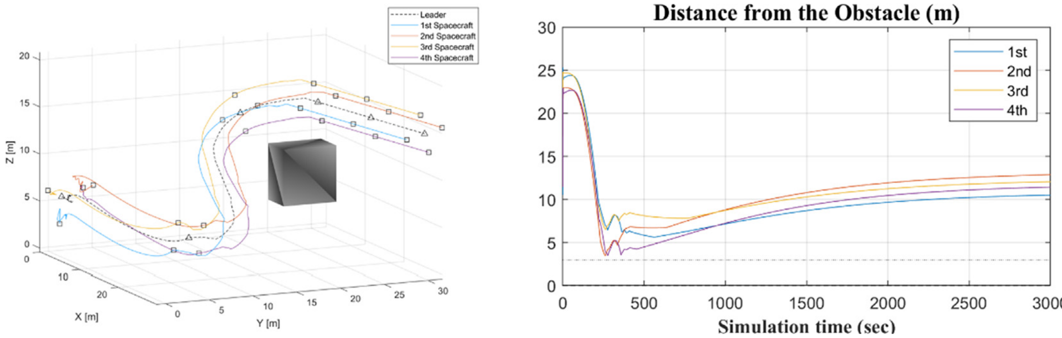

Fig. 8. Trajectory (Left) and Distances between four spacecraft and the obstacle (Right) with J_2 perturbation.

Table 2
Comparison of computation time and cost after employing J2 effects.

Method	Method C	Method C with J2 effect
Computation Time (sec)	1687.0	1778.4
Control Effort $\sqrt{\int u \cdot u^T dt}$ (m/sec)	(1st) 16.4294 (2nd) 14.0812 (3rd) 11.1174 (4th) 6.3174	(1st) 29.1913 (2nd) 25.4044 (3rd) 19.5912 (4th) 11.0471

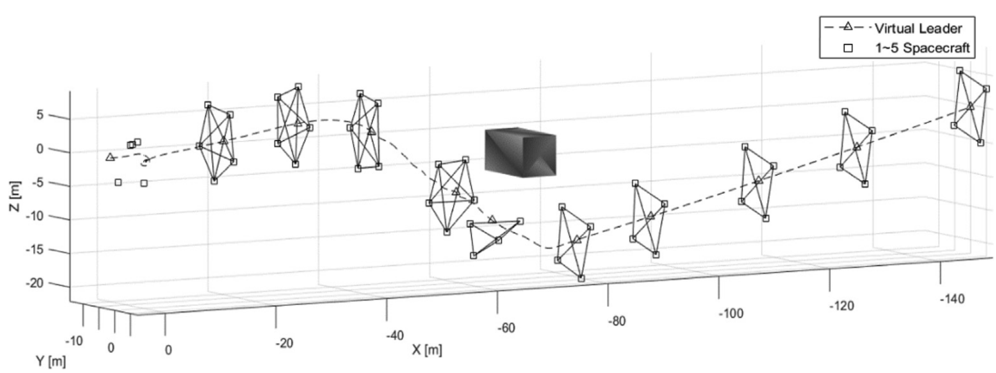

Fig. 9. Lines between four spacecraft (solid line), obstacle (grey face), reference trajectory of the virtual leader (dashed line), instantaneous position of virtual leader (Δ) and four spacecraft (□) at t = 150, 300, 450, 619, 670, 800, 1000, 1400, 2000, and 5000sec.

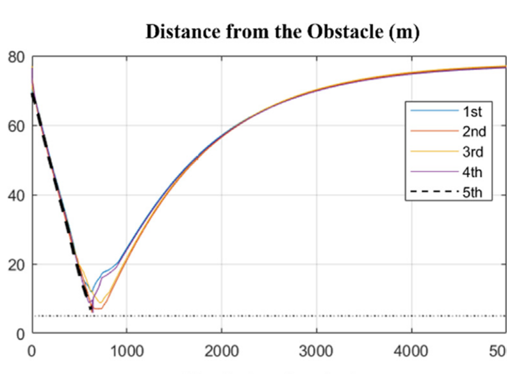

Fig. 10. Relative distances between obstacle and four spacecraft (solid line) and the fifth spacecraft (bold dotted line).

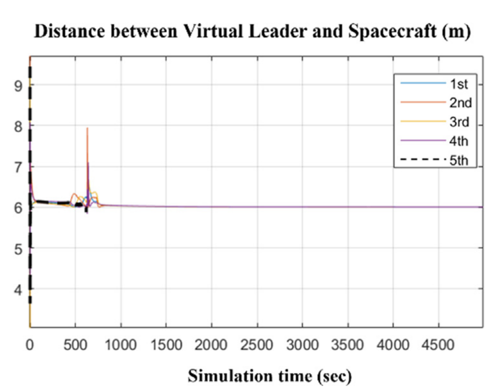

Fig. 11. Relative distances between virtual leader and five spacecraft (solid line) in pentagonal and square formation, the dashed line represents radius $R = 6m$ of the formation circle.

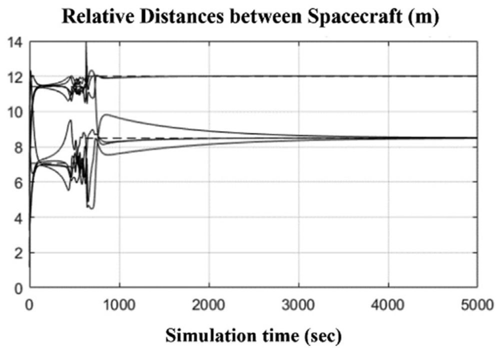

Fig. 12. Relative distances between five spacecraft (solid line), the dashed lines before 620 sec represent the side lengths 7.053m and diagonal length 11.413m of a regular pentagon, the dashed lines after 620 sec represent the side lengths 8.485m and diagonal 12m of square.

620 sec. It can be seen that the remaining four spacecraft without the fifth one successfully maintains their equidistant formation after 620 sec.

6. Conclusions

We have presented a novel and efficient approach for designing/controlling trajectories for spacecraft formation flying with collision avoidance. Based on the Artificial Potential Field (APF), the proposed controller synthesized the potentials for formation flying and collision avoidance in one single function, in which an *originally* derived rotational potential is incorporated in general *3-dimensional* space to avoid undesired convergence to a local minimum. The potential for formation, which consists of the structural and repulsive potentials, allows multiple spacecraft to maintain a regular polygonal shape and to autonomously reconfigure into another regular polygon in case some of them are broken or malfunctioning unexpectedly. The potential for collision avoidance incorporates the rotational potential in general 3-dimensional space to avoid local convergence.

The proposed controller has been first proven to be stable in the sense of Lyapunov, and successfully applied to three distinctive examples. In the first example, the proposed controller was able to drive a spacecraft to successfully avoid the local convergence to an undesired local minimum thanks to the rotational potential. In the second example, its performance to maintain the formation while avoiding collision has been favorably compared with the performance of an alternative approach. In the last example, the proposed controller was able to autonomously reconfigure the regular pentagonal formation into a square formation while avoiding collision.

These numerical illustrations imply that the proposed controller is competitive in terms of simplicity of formulation, formal proof in the sense of Lyapunov, efficient computation time and control efforts. With simple formulation and the associated low computational burden, the proposed APF-based approach may be suitable for formation flying with small satellites which have limited computation capacity.

Declaration of Competing Interest

The authors declare that they have no known competing financial interests or personal relationships that could have appeared to influence the work reported in this paper.

Acknowledgements

This research was supported by Basic Science Research Program through the National Research Foundation of Korea (NRF) funded by the Ministry of Education (2018R1D1A1B07045759, 2021R1I1A204882411), and by a grant from "Fundamental Research for Korea Satellite Navigation System and Future Air Traffic Management" of the Korea Aerospace Research Institute funded by the Korea government (MSIT).

References

Badawy, A., McInnes, C.R., 2008. On-orbit assembly using superquadric potential fields. J. Guidance, Control, Dynam. 31 (1), 30–43. https://doi.org/10.2514/1.28865.

Balch, T., Arkin, R.C., 1998. Behavior-based formation control for multirobot teams. IEEE Trans. Robot. Autom. 14 (6), 926–939. https://doi.org/10.1109/70.736776.

Bandyopadhyay, S., Foust, R., Subramanian, G.P., Chung, S.J., Hadaegh, F.Y., 2016. Review of formation flying and constellation missions using nanosatellites. J. Spacecraft Rockets 53 (3), 567–578. https://doi.org/10.2514/1.A33291.

Beard, R.W., Lawton, J., Hadaegh, F.Y., 2001. A coordination architecture for spacecraft formation control. IEEE Trans. Control Syst. Technol. 9 (6), 777–790. https://doi.org/10.1109/87.960341.

Burch, J.L., Moore, T.E., Torbert, R.B., Giles, B.L., 2016. Magnetospheric multiscale overview and science objectives. Space Sci. Rev. 199 (1–4), 5–21. https://doi.org/10.1007/s11214-015-0164-9.

Cao, L., Qiao, D., Xu, J., 2018. Suboptimal artificial potential function sliding mode control for spacecraft rendezvous with obstacle avoidance. Acta Astronaut. 143, 133–146. https://doi.org/10.1016/j.actaastro.2017.11.022.

Chai, R., Savvaris, A., Tsourdos, A., Chai, S., Xia, Y., 2019. A review of optimization techniques in spacecraft flight trajectory design. Prog. Aerosp. Sci. 109. https://doi.org/10.1186/s40064-016-2476-y 100543.

Chang, K., Xia, Y., Huang, K., 2016. UAV formation control design with obstacle avoidance in dynamic three-dimensional environment. SpringerPlus 5 (1), 1–16. https://doi.org/10.1186/s40064-016-2476-y.

Cheng, L., Wen, H., Jin, D., 2020. Reconfiguration control of satellite formation using online quasi-linearization iteration and symplectic discretization. Aerosp. Sci. Technol. 107. https://doi.org/10.1016/j.ast.2020.106348 106348.

Chu, X., Zhang, J., Lu, S., Zhang, Y., Sun, Y., 2016. Optimised collision avoidance for an ultra-close rendezvous with a failed satellite based on the Gauss pseudospectral method. Acta Astronaut. 128, 363–376. https://doi.org/10.2514/1.G002868.

Djojodihardjo, H., 2014. Influence of the earth's dominant oblateness parameter on the low formation orbits of micro-satellites. Int. J. Autom. Mech. Eng. 9, 1802. https://doi.org/10.15282/ijame.9.2013.28.0150.

Fu, X., Pan, J., Wang, H., Gao, X., 2020. A formation maintenance and reconstruction method of UAV swarm based on distributed control. Aerosp. Sci. Technol. 104. https://doi.org/10.1016/j.ast.2020.105981 105981.

Hu, Q., Dong, H., Zhang, Y., Ma, G., 2015. Tracking control of spacecraft formation flying with collision avoidance. Aerosp. Sci. Technol. 42, 353–364. https://doi.org/10.1016/j.ast.2014.12.031.

Hwang, J., 2019. Collision-Free Control for Formation Flying of Multiple Satellites Using Artificial Potential Field. Master's thesis. Yonsei University, Seoul, Republic of Korea.

Khatib, O., 1986. Real-time obstacle avoidance for manipulators and mobile robots. In: Autonomous robot vehicles. Springer, New York, NY, pp. 396–404. https://doi.org/10.1007/978-1-4613-8997-2_29.

Lee, D., Sanyal, A.K., Butcher, E.A., 2015. Asymptotic tracking control for spacecraft formation flying with decentralized collision avoidance. J. Guidance, Control Dynam. 38 (4), 587–600. https://doi.org/10.2514/1.G000101.

Li, Q., Yuan, J., Wang, H., 2018. Sliding mode control for autonomous spacecraft rendezvous with collision avoidance. Acta Astronaut. 151, 743–751. https://doi.org/10.1016/j.actaastro.2018.07.006.

Liu, X., Meng, Z., You, Z., 2018. Adaptive collision-free formation control for under-actuated spacecraft. Aerosp. Sci. Technol. 79, 223–232. https://doi.org/10.1016/j.ast.2018.05.040.

Pham, V.H., Trinh, M.H., Ahn, H.S., 2018. Formation control of rigid graphs with flex edges. Int. J. Robust Nonlinear Control 28 (6), 2543–2559. https://doi.org/10.1002/rnc.4037.

Ren, W., Sorensen, N., 2008. Distributed coordination architecture for multi-robot formation control. Rob. Auton. Syst. 56 (4), 324–333. https://doi.org/10.1016/j.robot.2007.08.005.

Rezaee, H., Abdollahi, F., 2013. A decentralized cooperative control scheme with obstacle avoidance for a team of mobile robots. IEEE Trans. Ind. Electron. 61 (1), 347–354. https://doi.org/10.1109/TIE.2013.2245612.

Roberts, J.A., Roberts, P.C., 2004. The development of high fidelity linearized J2 models for satellite formation flying control. AAS Paper, 04–162.

Rostami, S.M.H., Sangaiah, A.K., Wang, J., Liu, X., 2019. Obstacle avoidance of mobile robots using modified artificial potential field algorithm. EURASIP J. Wireless Commun. Netw. 2019 (1), 1–19. https://doi.org/10.1186/s13638-019-1396-2.

Rouzegar, H., Khosravi, A., Sarhadi, P., 2021. Spacecraft formation flying control around L2 sun-earth libration point using on–off SDRE approach. Adv. Space Res. 67 (7), 2172–2184. https://doi.org/10.1016/j.asr.2021.01.008.

Scharf, D.P., Hadaegh, F.Y., Ploen, S.R. (2004, June). A survey of spacecraft formation flying guidance and control. part ii: control. In Proceedings of the 2004 American control conference (Vol. 4, pp. 2976-2985). IEEE. https://doi.org/10.23919/ACC.2004.1384365.

Silvestrini, S., Lavagna, M., 2021. Neural-aided GNC reconfiguration algorithm for distributed space system: development and PIL test. Adv. Space Res. 67 (5), 1490–1505. https://doi.org/10.1016/j.asr.2020.12.014.

Starek, J.A., Açıkmeşe, B., Nesnas, I.A., Pavone, M., 2016. Spacecraft autonomy challenges for next-generation space missions. In: Advances in Control System Technology for Aerospace Applications. Springer, Berlin, Heidelberg, pp. 1–48. https://doi.org/10.1007/978-3-662-47694-9_1.

Steindorf, L.M., D'Amico, S., Scharnagl, J., Kempf, F., Schilling, K. (2017, February). Constrained low-thrust satellite formation-flying using relative orbit elements. In 27th AAS/AIAA Space Flight Mechanics Meeting (pp. 5–9).

Stilwell, D.J., Bishop, B.E., 2000. Platoons of underwater vehicles. IEEE Control Syst. Mag. 20 (6), 45–52. https://doi.org/10.1109/37.887448.

Wang, W., Baoyin, H., Mengali, G., Quarta, A.A., 2020. Solar sail cooperative formation flying around L2-type artificial equilibrium points. Acta Astronaut. 169, 224–239. https://doi.org/10.1016/j.actaastro.2019.10.028.

Warren, C. W. (1989, January). Global path planning using artificial potential fields. In 1989 IEEE International Conference on Robotics and Automation (pp. 316-317). IEEE Computer Society. https://doi.org/10.1109/ROBOT.1989.100007.

Wu, Y., Gou, J., Hu, X., Huang, Y., 2020. A new consensus theory-based method for formation control and obstacle avoidance of UAVs. Aerosp. Sci. Technol. 107. https://doi.org/10.1016/j.ast.2020.106332 106332.

Yang, C., Zhang, H., Gao, Y., 2021. Analysis of a neural-network-based adaptive controller for deep-space formation flying. Adv. Space Res. 68 (1), 54–70. https://doi.org/10.1016/j.asr.2021.03.007.